

Magneto- and Baro- Caloric Responses in Magnetovolumic Systems

Eduardo Mendive-Tapia

Department of Physics, University of Warwick, Coventry CV4 7AL, U.K.

Teresa Castán

Departament d'Estructura i Constituents de la Matèria.

Facultat de Física. Universitat de Barcelona. Diagonal, 647, E-08028 Barcelona, Catalonia.

(Dated: July 31, 2021)

Abstract

By means of a mean-field model extended to include magnetovolumic effects we study the effect of external fields on the thermal response characterized either by the isothermal entropy change and/or the adiabatic temperature change. The model includes two different situations induced by the magnetovolumic coupling. (i) A first order para- ferromagnetic phase transition that entails a volume change. (ii) An inversion of the effective exchange interaction that promotes the occurrence of an antiferromagnetic phase at low temperatures. In both cases, we study the magneto- and baro-caloric effects as well as the corresponding cross caloric responses. By comparing the present theoretical results with available experimental data for several materials we conclude that the present thermodynamical model reproduces the general trends associated with the considered caloric and cross caloric responses.

I. INTRODUCTION

Solid state refrigeration based on caloric effects is currently a very active research topic because of the possibility of developing new friendly alternative refrigeration devices¹. Caloric effects originate from the thermal response of every thermodynamic system to changes induced by the variation (either application or removal) of an external field². Depending on the external field, the corresponding caloric effect is called magnetocaloric (magnetic field)³⁻⁷, barocaloric (hydrostatic pressure)⁸⁻¹¹, electrocaloric (electric field)¹²⁻¹⁵, elastocaloric (mechanical stress)¹⁶⁻¹⁸, and toroidocaloric (toroidic field)¹⁹. The two limiting situations correspond to either varying the external field isothermically or adiabatically. In the first case a change in the entropy is induced while in the second the system responds with a temperature shift. These isothermal change of entropy and adiabatic change of temperature are commonly used in order to quantify the caloric response of a given system. The interest is to be able to induce a large caloric effect in response to small or moderate variations of the external field. Indeed, this is most likely to occur in the vicinity of a phase transition⁸. Moreover, systems with coupled degrees of freedom might respond to different species of external fields. This gives rise to the so called field-tune caloric effect and multicaloric effect²⁰⁻²³. In the first situation, the secondary field is kept constant during the variation of the primary field. While the primary field effectively drives the caloric response, the secondary field allows to adjust the best operative conditions. In the second situation, the multicaloric effect refers to the variation of two or more fields either simultaneously or sequentially. For instance, in the case of systems with magnetoelastic coupling, the interplay between magnetism and elastic properties allows to induce a caloric response in the system by the application of either a magnetic field or/and a mechanical field (hydrostatic pressure or stress). In the present investigation we shall focus in magnetovolumic systems.

Magnetovolumic effects arise as a special case of magnetoelastic coupling in which variations in the magnetization are accompanied by an isotropic change in volume. Such variations may be spontaneous, through a phase transition, or forced by the application of an external field. The interaction between volume and magnetism results in the interrelation between magneto- and baro- caloric effects observed experimentally in different materials²⁴⁻²⁸.

The present theoretical study is based on a mean-field Ising model²⁹ for phase transitions extended to include coupling between volume and magnetism. Interestingly, the model al-

lows to study two different situations. In the first one, the magnetovolumic coupling induces a first-order para-ferromagnetic phase transition that can be modified by the application of either a hydrostatic pressure or/and a magnetic field. In the second situation, the interplay between volume and magnetism originates a strong first-order antiferro-ferromagnetic transition that is responsive to the application of both hydrostatic pressure and magnetic field. Effective and mean-field approaches^{30–37} have been used previously to investigate magnetovolumic effects. Compared with these prior investigations, the present work incorporates the occurrence of a metamagnetic transition and the study of caloric and cross-caloric effects.

The paper is organized as follows. In section II we briefly resume the main aspects of the model and the thermodynamics of caloric effects. In section III and IV we solve numerically the model with special attention to the metamagnetic transition (section IV). We first obtain the phase diagram and study how the different transition temperatures change with applied fields (either hydrostatic pressure and/or magnetic field) and next we present the results for both the baro- and magneto- caloric effects. In section V we compare our results with experimental data available for magnetic and metamagnetic materials. We finally outline our main conclusions in section VI.

II. MODELING AND THERMODYNAMICS OF CALORIC EFFECTS

The model under consideration is based on the statistico-mechanical mean-field Ising model extended to include magnetovolumic effects. The starting point is a free-energy, consisting of the sum of two contributions, $f = f_M + f_C$. The first contribution, f_M , that accounts for the magnetic degrees of freedom, can be expressed in terms of both the ferromagnetic (m) and the antiferromagnetic (x) order parameters simultaneously²⁹

$$\begin{aligned} f_M(T, m, x) = & -\frac{Jz}{2}(m^2 - x^2) - k_B T \ln 2 + \frac{k_B T}{4}[(1 + m + x) \ln(1 + m + x) + \\ & + (1 + m - x) \ln(1 + m - x) + (1 - m + x) \ln(1 - m + x) + \\ & + (1 - m - x) \ln(1 - m - x)], \end{aligned} \quad (1)$$

Hereafter the exchange interaction is fixed to be positive ($J > 0$). In that case, the previous free energy (1) produces a continuous para-ferromagnetic phase transition at $T_c = zJ/k_B$, being z the number of nearest neighbours and k_B the Botzmann constant. The second contribution, f_C , incorporates the magnetovolumic coupling and includes magnetostriction

coupling of both order parameters, m and x , to the relative volume change $w = \frac{\delta\Omega}{\Omega}$, where Ω is some reference volume. Restricting the coupling terms to the minimum order allowed by symmetry, one may write:

$$f_C(m, x, w) = \frac{\alpha_0}{2}w^2 - (\alpha_1 m^2 + \alpha_2 x^2)\frac{w}{2}. \quad (2)$$

We have also included a purely elastic contribution, with α_0 being proportional to the inverse of the compressibility. Furthermore, in order to account for pressure effects as well as for the interplay with an external magnetic field, we introduce the following Legendre transform to the total free-energy:

$$g = f(T, m, x, w) - Hm + \Omega Pw, \quad (3)$$

where g stands for the Gibbs free-energy, P is the hydrostatic pressure and H is the external magnetic field. In expression (2) α_1 is the magnetostriction coefficient that gives rise to a first-order phase transition from a paramagnetic (\mathcal{P}) phase to a ferromagnetic (\mathcal{F}) phase when lowering the temperature. The coefficient α_2 causes an inversion-exchange of the effective interaction so that an antiferromagnetic (\mathcal{AF}) order might exist for some range of model parameters and applied external fields.

We remark that the Landau-based phenomenological expansion in eq. (2) is based on symmetry considerations and that it intends to describe the effects of the interplay between volume and magnetism rather than to address its physical origin. The physical mechanism that originates such interplay and the way it operates can be different from one system to another. Nevertheless, the symmetry-based coupling in (2) is present in all magnetic materials although in some cases can be negligible. Moreover, coupling coefficients are material dependent and can be functions of chemical composition and valence electron concentration, among others. It is worth mentioning that the linear-quadratic coupling between volume change and magnetization has been used previously through a prescribed linear dependence of the Curie temperature with the volume change³¹.

It is convenient to get rid of the (secondary) order parameter w by minimizing expression (3) with respect to w . One gets:

$$w = \frac{1}{2\alpha_0} [(\alpha_1 m^2 + \alpha_2 x^2) - 2P\Omega] \quad (4)$$

This constitutive equation verifies the following Maxwell relation^{21,38},

$$\left(\frac{\partial m}{\partial P}\right)_{T,H} = -\Omega \left(\frac{\partial \omega}{\partial H}\right)_{T,P}, \quad (5)$$

that underlines the origin of the multicaloric response. Therefore, the Gibbs free-energy per magnetic particle, in reduced units, along the optimum path involving m , x , and w given by (4), is:

$$\begin{aligned} g^* = \frac{g}{zJ} = & -\frac{1}{2}(m^2 - x^2) - T^* \ln 2 + \frac{T^*}{4}[(1+m+x) \ln(1+m+x) + \\ & + (1+m-x) \ln(1+m-x) + (1-m+x) \ln(1-m+x) + \\ & + (1-m-x) \ln(1-m-x)] - \frac{1}{8\alpha_0^*}[(\alpha_1^* m^2 + \alpha_2^* x^2) - 2P\Omega^*]^2 - H^* m. \end{aligned} \quad (6)$$

Where the superscript $(*)$ indicates that the magnitude is normalized to zJ . We take $\alpha_0^* = 1$, $\Omega^* = 1$, without loss of generality.

When a given external field (Y) is modified (applied/removed) isothermally, the corresponding caloric effect is related to the entropy change of the system that can be obtained from fundamental Thermodynamics^{6,38}. Indeed, for a finite change of the field ($Y = 0 \rightarrow Y \neq 0$), the corresponding field-induced isothermal entropy change will be given by:

$$\Delta S(T, 0 \rightarrow Y) = S(T, Y) - S(T, 0) = \int_0^Y \left(\frac{\partial S}{\partial Y} \right)_T dY = \int_0^Y \left(\frac{\partial X}{\partial T} \right)_Y dY, \quad (7)$$

where we have used the appropriate Maxwell relation and X is the thermodynamically conjugated variable to the field Y . The present model can be applied to study both magnetocaloric (MCE) and barocaloric (BCE) effects corresponding to ($Y = H$, $X = m$) and ($Y = -P$, $X = w$) respectively. Indeed, the entropy can be directly obtained from (6) by taking into account that,

$$\begin{aligned} S(m, x) = & - \left[\frac{\partial g^*}{\partial T^*} \right]_{H, P} = \\ & \ln 2 - \frac{1}{4}[(1+m+x) \ln(1+m+x) + (1-m+x) \ln(1-m+x) + \\ & + (1+m-x) \ln(1+m-x) + (1-m-x) \ln(1-m-x)] \end{aligned} \quad (8)$$

In the expression above, $m = m(T^*, H^*, P)$ and $x = x(T^*, H^*, P)$ are the equilibrium order parameters obtained after minimization of the free-energy (6). In addition, for a given caloric effect, the entropy change should depend on the (secondary) tuning field. For instance, the pressure-tune MCE at a given constant value of P , is characterized by the entropy difference $\Delta S(T, 0 \rightarrow H, P) = S(T, H, P) - S(T, 0, P)$. Alternatively, the magnetic field tuned BCE depends on the value of the (secondary) applied magnetic field H and it is given

by $\Delta S(T, H, 0 \rightarrow P) = S(T, H, P) - S(T, H, 0)$. Notice that by tuning the secondary field, it is possible to adjust the most optimum temperature range for the caloric effect. Moreover, in the case of the multicaloric effect the corresponding entropy change is given by $\Delta S(T, 0 \rightarrow H, 0 \rightarrow P) = S(T, H, P) - S(T, 0, 0)$ and both, pressure and magnetic field, are applied/removed simultaneously (or sequentially). Given that the entropy is a state function that depends only on the current state of the system, it is easy to show that⁷

$$\begin{aligned} \Delta S(T, 0 \rightarrow H, 0 \rightarrow P) &= \\ \Delta S_{MCE}(T, 0 \rightarrow H, 0) + \Delta S_{H-BCE}(T, H, 0 \rightarrow P) &= \\ \Delta S_{BCE}(T, 0, 0 \rightarrow P) + \Delta S_{P-MCE}(T, 0 \rightarrow H, P), \end{aligned} \quad (9)$$

where ΔS_{MCE} stands for MCE, ΔS_{P-MCE} for P-tune MCE, ΔS_{BCE} for BCE and ΔS_{H-BCE} for H-tune BCE. For the sake of clarity we shall keep this notation along the present work.

When the external field is changed adiabatically, the subsequent temperature change can be expressed as

$$\Delta T(0 \rightarrow Y) = - \int_0^Y \frac{T}{C} \left(\frac{\partial S}{\partial Y} \right)_T dY = - \int_0^Y \frac{T}{C} \left(\frac{\partial X}{\partial T} \right)_Y dY, \quad (10)$$

where again we have used the appropriate Maxwell relation. C is the heat capacity and the external field is varied from $Y = 0$ to $Y \neq 0$. Note that the previous thermodynamic expression (10) involves the total entropy of the system. Nevertheless, the model entropy in Eq. (8) only accounts for the magnetic contribution. Consequently, such entropy returns values for the calculated adiabatic temperature variations (10) definitively unphysical. To improve this, we consider the lattice contribution per particle in the Debye approximation, given by⁵

$$S_v = k_B \left[-3 \ln \left(1 - e^{-\frac{T}{\theta_D}} \right) + 12 \left(\frac{T}{\theta_D} \right)^3 \int_0^{\theta_D/T} \frac{x^3}{e^x - 1} dx \right], \quad (11)$$

θ_D being the Debye temperature. We now proceed by merely appending expression (11) to the magnetic entropy (8). Physically, this additional term plays the role of a thermal bath (or reservoir) replacing the effects of the remaining degrees of freedom not considered explicitly in the model. This is a quite usual approach in Statistical Mechanics. We notice that eventual influences due to a volume dependence of the lattice entropy contribution or electronic effects are not considered explicitly here. Nevertheless, when looking at the behaviour of a given specific material, such effects can be relevant and therefore should be taken into account.

III. FIELD-INDUCED FERROMAGNETIC TRANSITION

In this section we briefly summarize the main results obtained by solving numerically the minimal model that allows for a discontinuous \mathcal{P} -to- \mathcal{F} -phase transition, involving volume variation, under the application of an external field (either P or/and H). This corresponds to set $\alpha_2^*=0$ in eq.(6), obtaining the following free energy function:

$$g^* = -\frac{m^2}{2} - T^* \ln 2 + \frac{T^*}{2}[(1+m) \ln(1+m) + (1-m) \ln(1-m)] - \frac{1}{8\alpha_0^*}(\alpha_1^* m^2 + 2\Omega^* P)^2 - H^* m, \quad (12)$$

where the \mathcal{AF} order parameter is $x = 0$ for all range of T^* and α_1^* . For given values of the external fields, a further direct numerical minimization of (12) with respect to m renders the thermodynamical solutions for $m(T^*, H^*, P)$. Afterwards, it is possible to compute all thermodynamic quantities of interest. In the present study we restrict ourselves to some representative results. Firstly, figure 1 shows the phase diagram as a function of the coupling parameter α_1^* , for $H^*=0$ and for three different values of the pressure $P=0, 0.05, 0.1$, as indicated. Each curve exhibits two tricritical points $((\alpha_{1t}^*)_{\pm}, T_t^*)$ that change with the external pressure P . For $(\alpha_{1t}^*)_- < \alpha_1^* < (\alpha_{1t}^*)_+$ the transition is continuous whereas for $\alpha_1^* > (\alpha_{1t}^*)_+$ and $\alpha_1^* < (\alpha_{1t}^*)_-$ it is discontinuous. The Curie temperature T_c^* for the continuous transition³⁹ is given by $T_c^*(P^*) = 1 - \frac{\alpha_1^*}{\alpha_0^*} \Omega P$. An inspection of Fig.1 reveals that for $P = 0$ the sign of α_1^* is irrelevant whereas under the application of an external pressure, T_c^* (continuous line) may decrease or increase with P , depending on whether the coupling parameter α_1^* is positive or negative respectively. Beyond the tricritical points, the transition temperature for the first order transition (dashed line) increases with α_1^* , regardless its sign. Below, we summarize the main results obtained for the MCE and BCE behaviours for a representative value of $\alpha_1^* = \pm 1.10$, for which the transition is discontinuous.

Figure 2 displays the temperature behavior of the MCE for different external fields. In the upper panels we have plotted (a) the isothermal entropy change $\Delta S_{MCE}(T, 0 \rightarrow H^*, P = 0)$ and (b) the adiabatical temperature shift $\Delta T_a^*(0 \rightarrow H^*, P = 0)$, for increasing values of the applied magnetic field (denoted by an arrow). Both behaviours are consistent with a conventional MCE. To illustrate the behavior of the external pressure on the MCE, we have plotted the ΔS_{P-MCE} at $P = 0.05$ for $\alpha_1^* = 1.1$ (c) and $\alpha_1^* = -1.1$ (d). The effect of P is to shift the MCE peak either to lower (c) or higher (d) temperatures depending to sign of α_1^* ,

accordingly to the tendency of promoting the phase with lower volume.

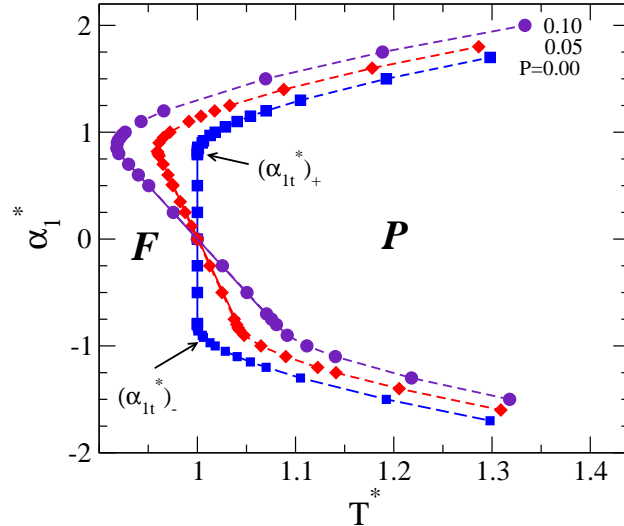


FIG. 1. (Color online) Transition temperature versus the coupling parameter α_1^* for $H^* = 0$. The three curves correspond to selected values of the pressure P as indicated. Second order transitions are denoted by solid lines whereas first order transitions by dashed lines. Both curves intersect at the two tricritical points $(\alpha_t^*)_+$ and $(\alpha_t^*)_-$.

The results for the BCE are shown in Fig. 3. As expected, one obtains different behaviors depending on the sign of α_1^* . Essentially, for $\alpha_1^* = 1.10$ the BCE is inverse whereas for $\alpha_1^* = -1.10$ it is conventional. Consequently, the entropy increases (a) or decreases (b) when the pressure is applied isothermally. Likewise, the system cools down (c) or warms up (d) when the pressure is applied adiabatically. The effect of H^* on the BCE is shown in the lower panels of the same figure for $\alpha_1^* = 1$ (e) and $\alpha_1^* = -1$ (f). As can be observed, the application of the secondary field H^* shifts the caloric response towards higher temperatures and reduces the peak, regardless of the sign of α_1^* . This reflects the natural tendency of the external H^* to promote the (ordered) \mathcal{F} -phase with lower entropy. In summary, the effect of increasing H^* on the BCE is to attain higher temperatures, at expenses of reducing the caloric response.

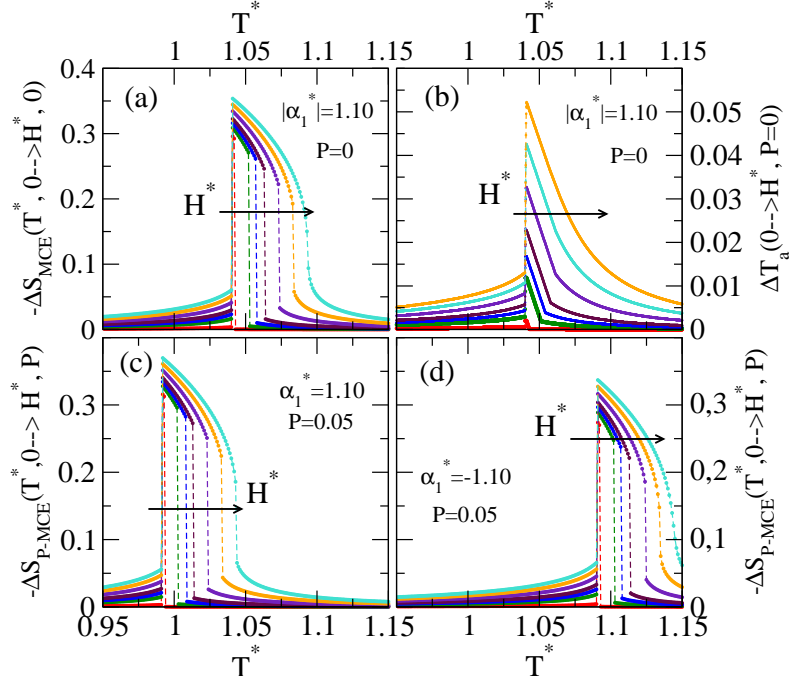


FIG. 2. (color online) MCE under the application of increasing values of the magnetic field H^* (denoted by an arrow). (a) Isothermal entropy change at $P = 0$, (b) adiabatic temperature change at $P = 0$, (c) and (d) isothermal entropy change at $P = 0.05$ for $\alpha_1^* = 1.10$ and $\alpha_1^* = -1.10$ respectively.

IV. THE METAMAGNETIC TRANSITION

The model for the metamagnetic transition corresponds to switch on the parameter α_2^* in the free-energy model defined in eq. (6). Notice that this parameter gives rise to an inversion in the effective exchange constant that renders the \mathcal{AF} stable at low temperatures. It is worth mentioning that the importance of magnetostriction in the occurrence of the $\mathcal{F} \rightarrow \mathcal{AF}$ metamagnetic transition was first pointed out by Kittel⁴⁰. For the following calculation we also take $|\alpha_1^*| = 1$ in order to favor discontinuous transitions. In that case, both order parameters, x and m , may be different from zero and the variation in the volume w will depend on the sign of both α_1^* and α_2^* . Standard numerical minimization of the reduced Gibbs free-energy (6) predicts the occurrence of an antiferromagnetic \mathcal{AF} -phase at low temperatures, as it can be seen in the phase diagram shown in Fig. 4(a). In this figure we have plotted the behavior (in absence of external fields) of the different transition

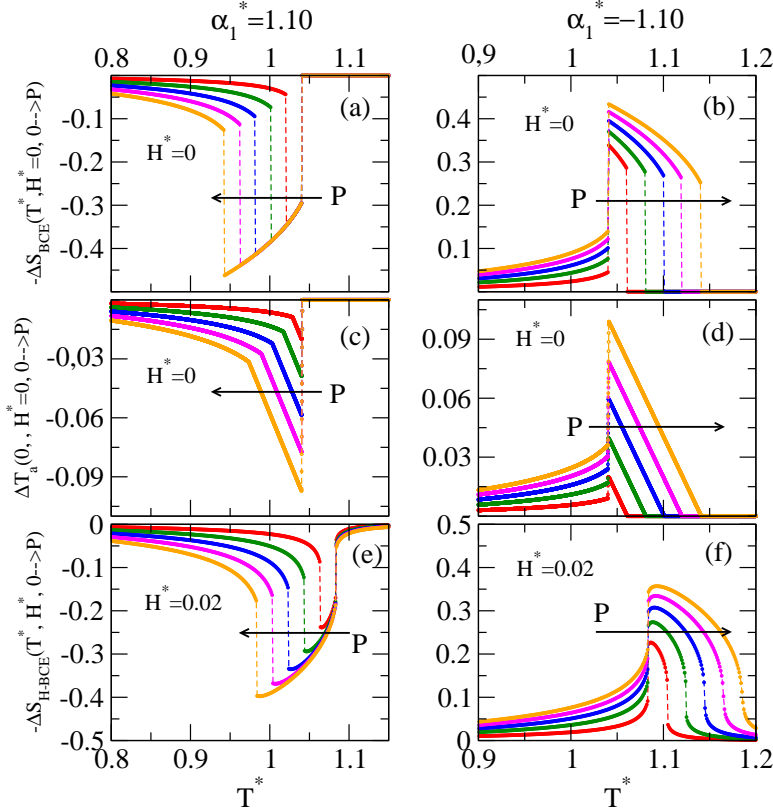


FIG. 3. (Color online) BCE for two representative values of $\alpha_1^* = 1.10$ (left column) and $\alpha_1^* = -1.10$ (right column) for increasing values of the applied pressure P^* . Panels (a) and (b) display the isothermal entropy change at $H^* = 0$, (c) and (d) the corresponding adiabatic temperature shift and (e) and (f) the isothermal entropy change at $H^* = 0.02$.

temperatures as a function of the coupling parameter α_2^* restricted to positive values for the sake of clarity⁴¹. That is, the Curie temperature T_C^* (\mathcal{P} - \mathcal{F}), the Neel temperature T_N^* (\mathcal{P} - \mathcal{AF}) and the metamagnetic transition temperature T_M^* (\mathcal{AF} - \mathcal{F}). The \mathcal{AF} -phase exists only for values of the coupling parameter $\alpha_2^* > \alpha_{2c}^*$, where α_{2c}^* satisfies⁴²:

$$(\alpha_{2c}^*)^2 - (\alpha_1^*)^2 - 4\Omega^*P(\alpha_{2c}^* - \alpha_1^*) - 8\alpha_0^*(1 + H^*) = 0 \quad (13)$$

The temperature range at which the \mathcal{AF} -phase exists increases with the coupling strength α_2^* . There is a particular value, α_{2t}^* , at which the three phases \mathcal{P} , \mathcal{F} and \mathcal{AF} coexist. Thus, for $\alpha_{2c}^* < \alpha_2^* < \alpha_{2t}^*$, the model predicts two consecutive phase transitions whereas for $\alpha_2^* > \alpha_{2t}^*$ the \mathcal{F} -phase disappears and the model exhibits an unique \mathcal{P} -to- \mathcal{AF} -phase transition at T_N^* .

Let us focus on the region of the phase diagram where the metamagnetic transition exists and take $|\alpha_2^*| = 3.05$ (green line in Fig. 4(a)). In the lower panels of Fig.4 we show the

corresponding behavior of both transition temperatures, T^*_C and T^*_M , with applied external P (b) for $\alpha_2^* = 3.05$ and (c) $\alpha_2^* = -3.05$ respectively. In both cases we explicitly distinguish between $\alpha_1^* = 1$ (blue) and $\alpha_1^* = -1$ (red). One observes that whereas for $\alpha_2^* = 3.05$ the application of P tends to suppress the \mathcal{AF} -phase rapidly, for $\alpha_2^* = -3.05$ the application of P definitively renders the \mathcal{AF} -phase favorable. Interestingly, the behavior displayed in Fig. 4 (b) and (c) embodies whether the BCE is conventional (increasing transition temperature with increasing P) or inverse (decreasing transition temperature with increasing P). In Fig.

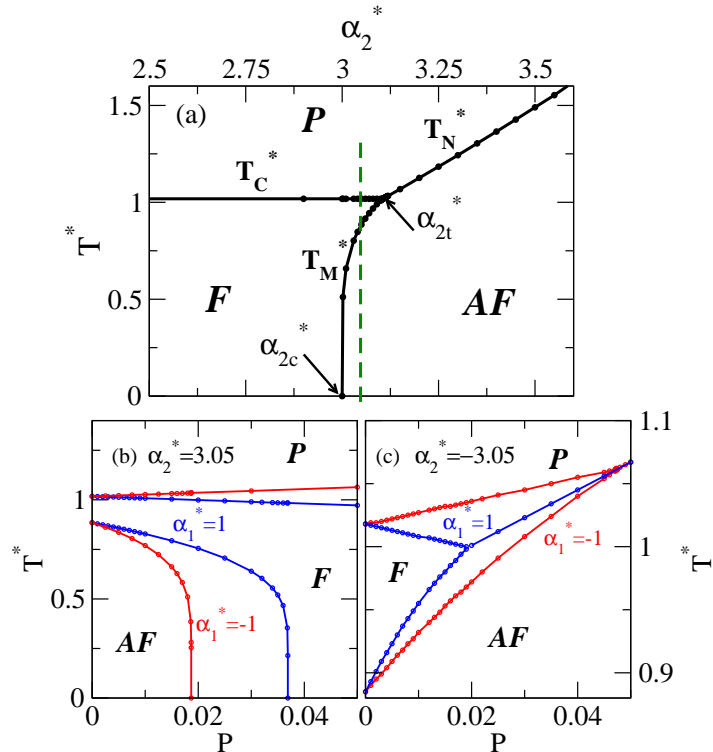


FIG. 4. (Color online) (a) Phase diagram for the exchange-inversion model in the region of positive α_2^* at $H^* = 0$, $P = 0$ and $\alpha_1^* = 1$. The green dashed line denotes the value of $\alpha_2^* = 3.05$ set for the present calculations. Lower panels show the pressure behavior of the corresponding transition temperatures T_C^* and T_M^* in the case of $\alpha_2^* = 3.05$ (b) and $\alpha_2^* = -3.05$ (c). Results are shown distinctly for $\alpha_1^* = 1$ (blue) and $\alpha_1^* = -1$ (red).

5 we show the MCE at different values of H^* ranging from $H^* = 0$ to $H^* = 0.04$. The increasing stability of the \mathcal{F} -phase is reflected in the decrease of T_M^* and the simultaneous increase of T_C^* with increasing H^* . In connexion with this, near the \mathcal{P} -to- \mathcal{F} transition (T_C^*), the MCE is conventional while it is inverse at lower temperatures, around the \mathcal{F} -to- \mathcal{AF}

transition (T_M^*). Moreover, the conventional MCE peak increases with H^* whereas the inverse MCE peak decreases. This apparent contradiction regarding the behavior of the inverse MCE around the \mathcal{F} -to- \mathcal{AF} transition has to do with the opposite effect that the application of H^* has on the entropy of both \mathcal{F} - and \mathcal{AF} - phases. In this sense, the model predicts a sharp suppression of the \mathcal{AF} -phase that hinders a further increase of the entropy with increasing H^* . To complete the discussion on the MCE, it is worth mentioning that, in adiabatic conditions, the system will first warm up (at high temperatures) and next cool down (at low temperatures) with the application of external H^* .

The effect of an external P on the MCE is displayed in the next figure 6 where we have plotted the corresponding isothermal entropy change at $P = 0.015$ and selected values of the applied magnetic field ranging from $H^* = 0$ to $H^* = 0.05$. Results have been calculated for the different values $\alpha_2^* = \pm 3.05$ and $\alpha_1^* = \pm 1$ considered previously. In general, the effect of the secondary field is a temperature shift in the corresponding caloric peak. As already mentioned, such displacement along the temperature axis should be consistent with the behavior of the transition temperatures displayed in figures 4(b) and 4(c). Indeed, an inspection of Fig. 6 reveals that for $\alpha_2^* = 3.05$ the effect of P on the inverse MCE peak (around T_M^*) is a shift to lower temperatures and a decay in the response whereas for $\alpha_2^* = -3.05$ the response gets enhanced and shifted to higher temperatures. Notice that for $\alpha_1^* = -1$ the effect is dramatic since the application of P induces a further promotion of the \mathcal{F} -phase. Regarding to the behavior of the conventional MCE around T_C^* , it has been already discussed before. Similarly, the temperature shift in the peaks follow the trends described in Fig. 4(b) and (c).

The results for the BCE behavior are shown in the next figure 7 for the same values of the coupling parameters. The isothermal entropy change ΔS_{BCE} is displayed for selected values of the applied pressure ranging from $P = 0$ to $P = 0.035$. Whereas the characteristics (whether it is inverse or conventional) of the high temperature peak around the \mathcal{P} - \mathcal{F} transition depends on the sign of α_1^* , α_2^* determines the characteristics of the low temperature peak around the metamagnetic transition. Thus, for $\alpha_2^* = 3.05$ (panels (a) and (b)) the BCE around T_M^* is inverse due to the suppression of the \mathcal{AF} -phase with increasing the applied pressure P (Fig. 4 (b)). Similarly, in the case of $\alpha_2^* = -3.05$ the low-temperature BCE is conventional. Furthermore, with increasing P , the BCE peak gets larger for $\alpha_1^* = 1$ and smaller for $\alpha_1^* = -1$. This is due to the fact that for positive α_1^* the application of P favors

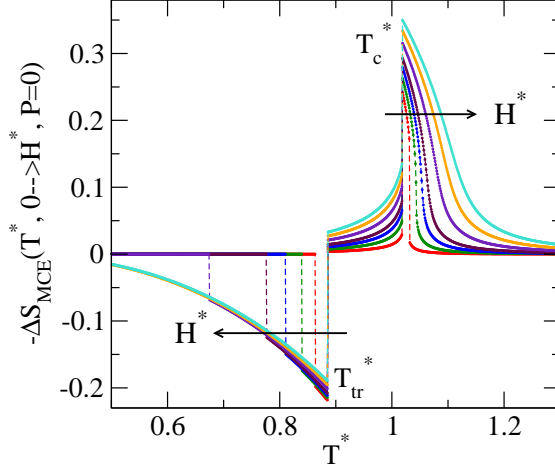


FIG. 5. (Color online) MCE for different values of the external magnetic field ranging from $H^* = 0$ to $H^* = 0.05$. T_C^* and T_M^* denote the \mathcal{P} -to- \mathcal{F} and \mathcal{F} -to- \mathcal{AF} transition temperatures respectively. As usual, the arrow denotes the direction of increasing H^* .

the disordered \mathcal{P} -phase (in detriment of the \mathcal{F} -phase, with larger volume) while for negative values of α_1^* the ordered \mathcal{F} -phase is promoted. Concerning the second BCE peak around T_C^* , it is inverse for $\alpha_1^* = 1$ and conventional for $\alpha_1^* = -1$, consistently with the behavior of T_C^* vs. P shown in figures 4(b) and 4(c).

To complete this section, in the different panels of figure 8 we have included the effect of the secondary field ($H^* = 0.02$) on the previous BCE. A simple comparison with Fig. 7 reveals that the effect of applying a magnetic field is to move away one peak from the other and simultaneously to decrease the caloric response, regardless of the model parameters. In summary, the application of H^* systematically reduces the response of the BCE and increases the stability of the (\mathcal{F}) phase.

V. RELATION TO EXPERIMENTS

In this section we analyze the previous theoretical results in relation to the different caloric behaviors observed in magnetic and metamagnetic materials for which experimental data is available. We stress that discussion on the physical origin or mechanism behind the magnetoelastic coupling is out of the scope here. Rather, we shall just require that the observation of the magnetic phase transition be accompanied by some volume anomaly. Below, we appraise our model predictions, namely phase diagram and caloric responses, by

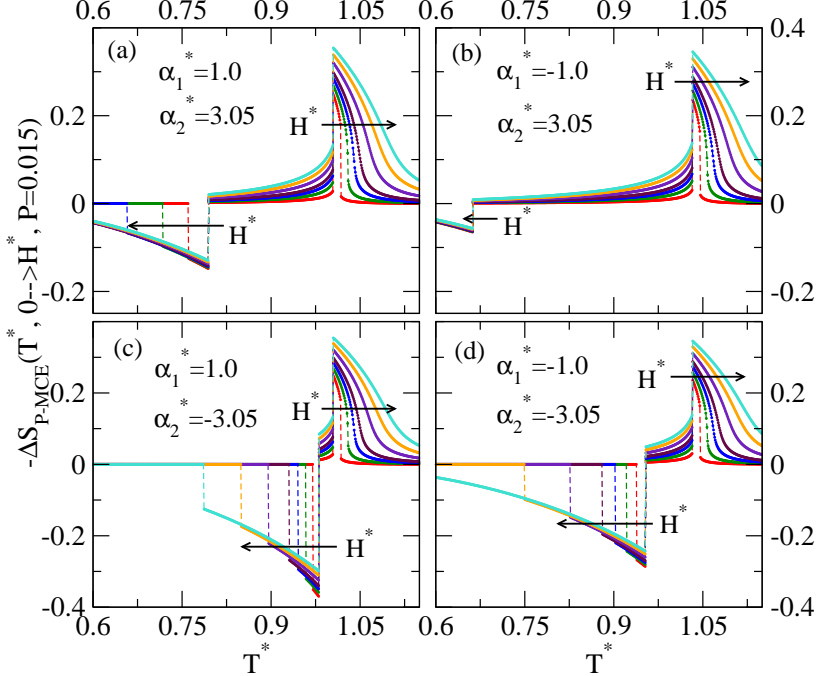


FIG. 6. (Color online) P-tune MCE for values of the applied external field ranging from from $H^* = 0$ to $H^* = 0.05$ and $P = 0.015$. Results are displayed distinctly for $\alpha_1^* = \pm 1$ and $\alpha_2^* = \pm 3.05$.

comparing them with experiments in the case of two potential magnetic refrigerant materials, $La_{(1-x)}Ca_xMnO_3$ and $FeRh$. Qualitative information regarding general aspects such as whether the caloric effect is conventional or inverse and the behavior (i.e. the temperature shift) of the caloric peak under the application of a secondary field can be inferred directly from the phase diagram. Even so, the maximum value of the caloric response, either on ΔS_T or ΔT_a might depend on other aspects or contributions not described properly (or not described) in the model.

A. The $La_{(1-x)}Ca_xMnO_3$ CMR system

Few years ago, very much attention was given to the study of the $La_{(1-x)}Ca_xMnO_3$ perovskite because of the unexpected large magnetoresistance observed at low temperatures⁴³. As a function of temperature and doping (x), this material shows different magnetic transitions⁴⁴. When lowering the temperature, it exhibits a $\mathcal{P} \rightarrow \mathcal{F}$ transition for $x \leq 0.50$ and a $\mathcal{P} \rightarrow \mathcal{AF}$ transition for $x \geq 0.5$. From the point of view of the present model, such a different magnetic behavior can be taken into account by recalling that both coupling

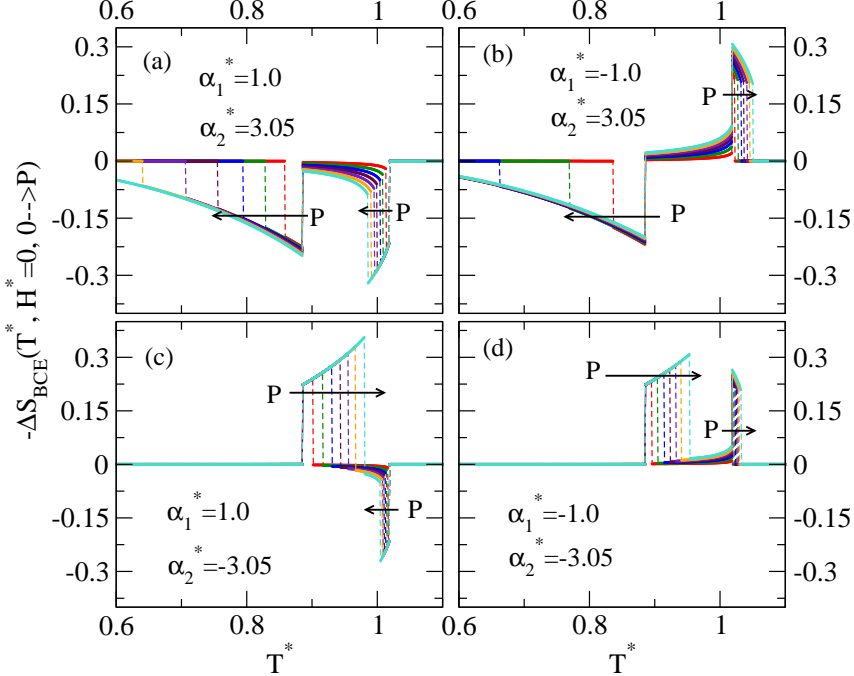


FIG. 7. (Color online) ΔS_{BCE} for increasing selected values of the applied pressure ranging from $P = 0$ to $P = 0.035$. Results are displayed distinctly for $\alpha_1^* = \pm 1$ and $\alpha_2^* = \pm 3.05$.

coefficients, α_1^* and α_2^* , are composition dependent. In figure 9 we present the results obtained for the transition temperature assuming a quadratic dependence with doping for both coefficients. The present numerical results (denoted by a continuous line) have been obtained by taking $\alpha_1^* = 24.22(x - 0.38)^2 - 2.5$ and $\alpha_2^* = -22.45(x - 0.64)^2 + 3.8$. The corresponding estimation for the exchange constant is $zJ = 16.6\text{meV}$, close to the values (6.6-10.7) meV reported in the literature⁴⁵. The model results are compared with available experimental data taken from different authors, as indicated in the inset. We might conclude that the agreement is remarkable. The unusual deviation around $x \sim 30\%$ is attributed⁴⁶⁻⁴⁹ to differences in the method used in preparing the sample. Interestingly, close to $x \sim 0.50$ the ground state changes from \mathcal{F} to \mathcal{AF} although the direct $\mathcal{F} \rightarrow \mathcal{AF}$ metamagnetic transition (if possible) will be restricted to a very narrow interval of values of x . Actually, metamagnetic transitions in $La_{(1-x)}Ca_xMnO_3$ have only been reported under the application of (low) external magnetic fields⁵⁰.

Moreover, perovskite manganites show a strong spin-lattice coupling⁵¹. This makes the study of pressure effects on their magnetic behavior of potential interest. In fig. 10 we show the effect of pressure on the MCE in $La_{0.69}Ca_{0.31}MnO_3$. Panel (a) displays the experimental

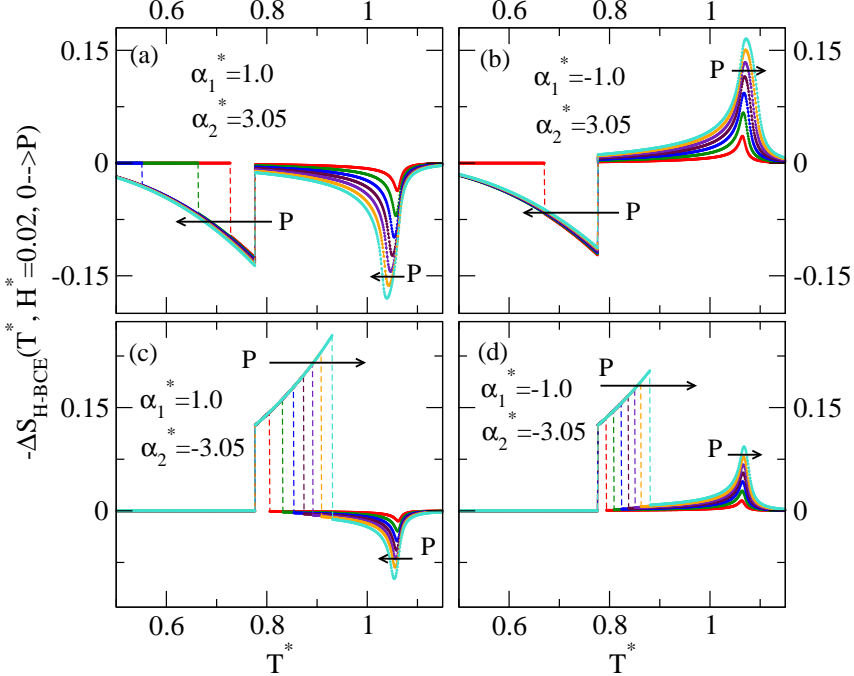


FIG. 8. (Color online) ΔS_{H-BCE} for increasing values of the applied pressure from $P = 0$ to $P = 0.035$ and $H^* = 0.02$. Results are displayed distinctly for $\alpha_1^* = \pm 1$ and $\alpha_2^* = \pm 3.05$.

data⁴⁷ for different values of the applied magnetic field and for two values of the applied pressure, $P \approx 0$ (ambient pressure) and $P = 1.1\text{GPa}$. In panel (b) we have plotted the present numerical results obtained for $\alpha_1^* = -2.38$ and $\alpha_2^* = 1.36$ and for the same values of the fields as in panel (a). We obtain an estimation for the volume of the unit cell of $\Omega \approx 29(\text{\AA})^3$, one half of the experimental value^{45,52} ($\sim 60(\text{\AA})^3$) but with the right order of magnitude. Before continuing with the discussion of fig. 10, let us point out that for these values of the coupling coefficients, $|\alpha_2^*| < |\alpha_{2c}^*|$ (defined in eq. (13)). The model predicts an unique $\mathcal{P} \rightarrow \mathcal{F}$ transition at a temperature that increases with both applied magnetic field and pressure. In this situation, the parameter α_2^* is irrelevant and consequently the description can be done by means of the simplified model defined in section III, with $\alpha_1^* < 0$. Indeed, our results preview that both MCE (fig. 2 (a) and (b)) and BCE (fig. 3 (b) and (d)) are conventional with behavior under external fields given in figures 2(d) and 3(f). We now return to figure 10. A simple inspection reveals that in this material the main effect of pressure on the MCE is a simple shift of the whole response (almost unaltered) to higher temperatures consistently with the increasing stability of the \mathcal{F} -phase (with lower volume) with P . In conclusion, the model is able to reproduce the general experimental

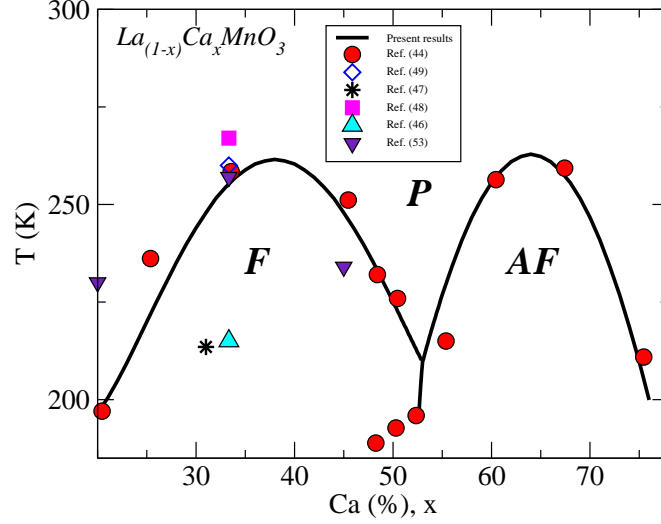


FIG. 9. (Color online) Phase Diagram for $La_{1-x}Ca_xMnO_3$ as a function of the Ca content (x). Continuous line denotes the present numerical results obtained by assuming a quadratic dependence of the coupling parameters α_1^* and α_2^* with doping x . Points correspond to experimental data from different authors indicated in the inset.

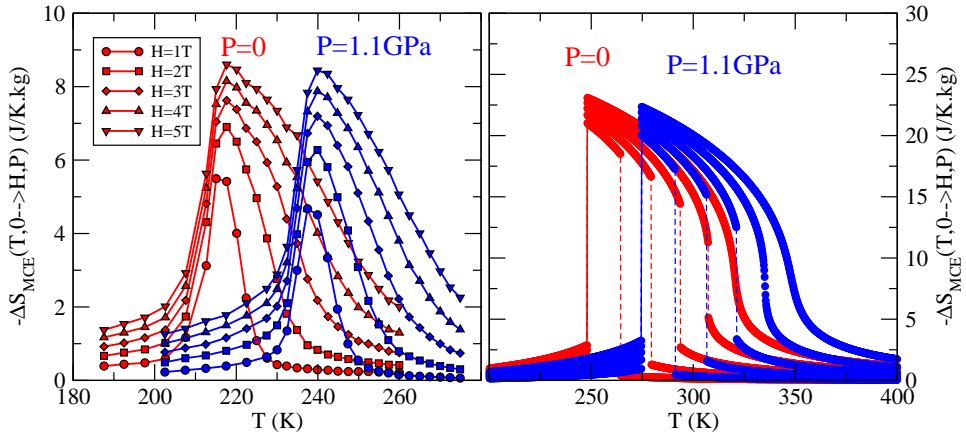


FIG. 10. (Color online). Effect of the pressure on the ΔS_{MCE} in $La_{0.69}Ca_{0.31}MnO_3$. (a) corresponds to experimental data taken from Ref.(47) and (b) displays the present numerical results for the same values of applied fields and pressures.

trends. Nevertheless, the amount of ΔS_{MCE} even though has the right order of magnitude is underestimate by a factor two (roughly). We attribute this to other entropy contributions, mainly electronic, not considered in the present model.

Very briefly we would like to mention that similar behavior is observed in $La(Fe_xSi_{1-x})_{13}$

-type compounds. The field-induced first-order \mathcal{P} -to- \mathcal{F} phase transition when lowering the temperature, is accompanied by a significant isotropic expansion of the volume and the application of an external P reduces the Curie temperature²⁶. Again, the description of the general trends can be done by the simplified model (12) but now with $\alpha_1^* > 0$. It has been reported that the MCE is conventional^{9,24,53} whereas the BCE is inverse⁹. Indeed, results shown in figures 2(a) and 3(a) are consistent with such experimental behavior. Additionally, the tuning of the MCE by an external pressure shifts the whole caloric effect towards lower temperatures²⁶ and the BCE exhibits a negative adiabatic temperature change⁹. These trends are reproduced in figures 2(c) and 3(c).

B. The FeRh metamagnetic alloy

The $B2$ ordered near-equiautomic $Fe_{1-x}Rh_x$ alloy displays a metamagnetic transition from an \mathcal{AF} ground state to a \mathcal{F} -phase with increasing temperature. It occurs around $T \sim 320K$ and it is accompanied by a 1% volume increasing in the unit cell that preserves the cubic symmetry^{18,54–56}. This singular transition is strongly concentration dependent⁵⁷ and it is only present for a very narrow range of the composition ($0.48 \leq x \leq 0.52$)⁵⁶. Additionally, it also depends on heat treatment²⁷, configurational ordering^{57,58} and external fields. Of special interest is the study of pressure effects on the magnetic behavior^{59–63}. The \mathcal{F} -phase, in between the \mathcal{P} -phase (at high temperatures) and the \mathcal{AF} -phase (at low temperatures), exists only for values of the applied pressure below ~ 6 GPa (tricritical pressure). For higher pressures the metamagnetic transition disappears and the \mathcal{AF} -phase transforms into the \mathcal{P} -phase directly. In the next figure 11 we show the P - T phase diagram for the nominally equiautomic $Fe_{(1-x)}Rh_x$ ($x \approx 0.5$). Continuous (blue) lines denote the present results for $\alpha_1^* = 1$ and $\alpha_2^* = -3.0$ (see fig. 4) whereas points correspond to experimental data taken from different authors indicated in the inset. The fitting to the experimental data renders the following estimations $zJ = 5.66\text{meV}$ and $\Omega = 36(\text{\AA})^3$, comparable to recently reported values for the exchange constant⁶⁴ and the lattice parameter⁵⁶ respectively. The misfit between theory and experiments ($\sim 10\%$ around the tricritical point) is partially due to the more attention given in the fitting procedure at the behavior close to $P=0$. In spite of this, we conclude that the agreement is satisfactory.

Concerning the caloric behavior in $FeRh$ metamagnetic alloy near the \mathcal{F} - \mathcal{AF} transition,

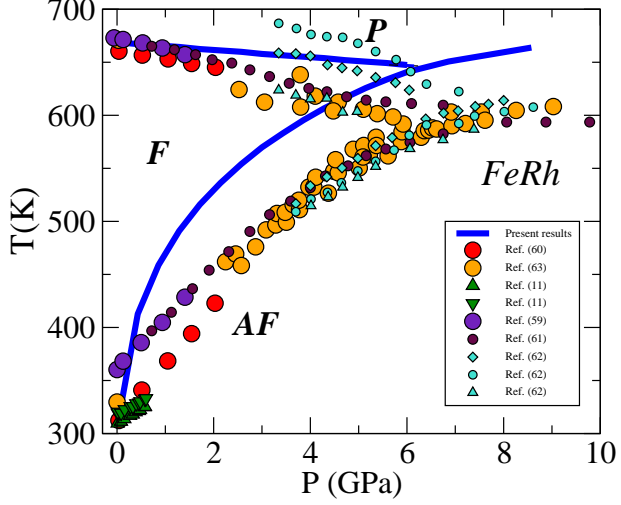


FIG. 11. (Color online) P - T phase diagram for the equiatomic $FeRh$ alloy. The present numerical results (blue line) are compared with available experimental data taken from different authors indicated in the inset.

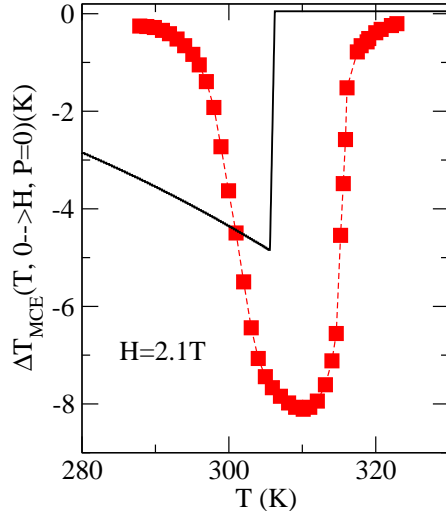


FIG. 12. (Color online) Adiabatic temperature change in the MCE at $H=2.1T$ in $FeRh$ alloy. Symbols correspond to experimental data from Ref. (27) whereas the continuous line indicate the present results.

experiments show that the MCE is inverse^{11,27} while the BCE is conventional¹¹. Under the application of an external pressure this transition temperature increases while the Curie temperature decreases⁶⁰. This scenario is reproduced by the present theoretical predictions shown in figures 6 (c) and 7(c). In Figure 12 we show the cooling by the adiabatic mag-

netization (as expected for an inverse MCE) as observed near the metamagnetic transition in *FeRh*. Experiments²⁷ are denoted by symbols whereas the continuous line corresponds to our results. These last have been obtained from the entropy curves by requiring that $S(T_f, H = 2.1T, P = 0) = S(T, 0, 0)$ and using $\Theta_D = 400K$. Experimentally, the maximum cooling at $H = 2.1T$ is of $\Delta T_{exp} = -8K$ whereas we obtain $\Delta T = -4.9K$.

Unfortunately the present model predicts a value for the entropy change (either in the MCE or BCE) in *FeRh* one order of magnitude below the experimental value^{11,27} ($|\Delta S_{exp}| = 12JK^{-1}Kg.^{-1}$). Principally this is due to the subtle balance between the different entropy contributions⁶⁵ ΔS_{mag} (magnetic), ΔS_v (lattice) and ΔS_{elec} (electronic) and the crucial role played by this last in ensuring a large enough value for the total amount of the entropy change. Although still under debate, it is accepted that in *FeRh* the $\mathcal{AF} \rightarrow \mathcal{F}$ metamagnetic transition is driven by an excess of electronic and magnetic entropy while the lattice opposes to the transition. Roughly speaking $\Delta S_v \approx -70\% \Delta S_{mag}$ and ΔS_{elec} represents a 40% of the total ΔS . This balance makes our model- that does not consider the electronic contribution- unqualified to obtain a reasonable value of the entropy change in this material. Nevertheless it predicts a quite acceptable value for the adiabatical temperature change due to the satisfactory description of the *P-T* phase diagram. In this regard, it should be mentioned that completely adiabatic conditions are very difficult to achieve experimentally. Finally let us noting a recent study⁵⁶ aimed at finding out magnetostructural trends in FeRh-based alloys. In particular, the behavior of the transition temperature as a function of the valence electron per atom seems to confirm the importance of the electronic effects on the transition. Also, these results seem to indicate that magnetovolumic effects are not essential for the transition although they are crucial in stabilizing the low temperature \mathcal{AF} -phase.

VI. CONCLUSIONS

We present a mean-field Landau-based model for phase transitions that captures the main ingredients necessary to reproduce the phase diagram and the general trends of the experimental caloric behavior observed in magnetoelastic materials in response to the application of external fields, either magnetic or/and hydrostatical pressure. In particular, we have applied the results to *LaCaMnO₃* perovskite and to *FeRh* metamagnetic alloy. Such

materials are very different but have the common feature of undergoing a magnetic phase transition accompanied by magnetoelastic effects. This is enough for the model to be able to reproduce both phase diagrams to a very good level of agreement with the experiments. The main limitation of the model is to predict the correct order of magnitude for the entropy change at the metamagnetic transition. Apparently, this is due to the fact that it includes the magnetic degrees of freedom only disregarding the role of the electronic contribution that in this material turns out to be very important. Concerning the lattice contribution, it plays the role of a thermal bath for the adiabatic caloric process. In this sense, Gruner *et al.*, by performing Monte Carlo simulations of a spin-based model extended to include magnetovolumic effects, were able to obtain a value for the entropy change within the range of the experimental results⁵⁵. This could be indicative of the importance of fluctuations in the occurrence of metamagnetic transitions. Additionally, coupling coefficients can be evaluated from first principle calculation thus providing an estimation independent on the model.

ACKNOWLEDGMENTS

This work has received financial support from CICYT (Spain), Project No. MAT2013-40590-P. One of us (E.M.) thanks the Spanish Ministry of Education, Culture and Sports for the fellowship for collaboration with the Dept. d'Estructura i Constituents de la Materia (UB) during his last year of undergraduate student in Physics.

¹ K. Sandeman, Scr. Mater. **67**, 566 (2012).

² L. Mañosa, A. Planes, and M. Mehmet, J. Mater. Chem. A **1**, 4925 (2013).

³ T. Krenke, E. Duman, M. Acet, E. Wassermann, X. Moya, L. Mañosa, and A. Planes, Nature Mater. **4**, 450 (2005).

⁴ K. G. Sandeman, R. Daou, S. Özcan, J. H. Durrell, N. D. Mathur, and D. J. Fray, Phys. Rev. B **74**, 224436 (2006).

⁵ N. de Oliveira and P. von Ranke, Phys. Rep. **489**, 89 (2010).

⁶ A. Planes, L. Mañosa, and M. Acet, J. Phys.: Condens. Matter. **21**, 233201 (2009).

⁷ A. Planes, L. Mañosa, and M. Acet, *Magneto and Mechanocaloric effects in Heusler alloys* (John Wiley & Sons, N.Y., 2015).

⁸ L. Mañosa, D. Gonzalez-Alonso, A. Planes, E. Bonnot, M. Barrio, J. Tamarit, S. Aksoy, and M. Acet, *Nature Mater.* **9**, 478 (2010).

⁹ L. Mañosa, D. Gonzalez-Alonso, A. Planes., M. Barrio, J. Tamarit, I. Titov, M. Acet, A. Bhat-tacharyya, and S. Majumdar, *Nat. Commun.* (2011), DOI:10.1038/ncomms1606.

¹⁰ N. de Oliveira, *J. Appl. Phys.* **109**, 053515 (2011).

¹¹ E. Stern-Taulats, A. Planes, P. Lloveras, M. Barrio, J. L. Tamarit, S. Pramanick, S. Majumdar, C. Frontera, and L. Mañosa, *Phys. Rev. B* **89**, 214105 (2014).

¹² B. Neese, B. Chu, S.-G. Lu, Y. Wang, E. Furman, and Q. M. Zhang, *Science* **321**, 821 (2008).

¹³ S. G. Lu, B. Rožič, Q. M. Zhang, Z. Kutnjak, and B. Neese, *Appl. Phys. Lett.* **98**, 122906 (2011).

¹⁴ X. Moya, E. Stern-Taulats, S. Crossley, D. González-Alonso, S. Kar-Narayan, A. Planes, L. Mañosa, and N. Mathur, *Adv. Mater.* **25**, 1360 (2013).

¹⁵ S. Lisenkov, B. K. Mani, C. M. Chang, J. Almand, and I. Ponomareva, *Phys. Rev. B* **87**, 224101 (2013).

¹⁶ E. Bonnot, R. Romero, L. Mañosa, E. Vives, and A. Planes, *Phys. Rev. Lett.* **100**, 125901 (2008).

¹⁷ F. Xiao, T. Fukuda, and T. Kakeshita, *Appl. Phys. Lett.* **102**, 161914 (2013).

¹⁸ S. Nikitin, G. Myalikgulyev, M. Annaorazov, A. Tyurin, R. Myndyev, and S. Akopyan, *Phys. Lett. A* **171**, 234 (1992).

¹⁹ T. Castán, A. Planes, and A. Saxena, *Phys. Rev. B* **85**, 144429 (2012).

²⁰ S. Fähler, U. Rößler, O. Kastner, J. E. G. Eggeler, H. Emmerich, P. Entel, S. Müller, E. Quandt, and K. Albe, *Adv. Eng. Mat.* **14**, 10 (2012).

²¹ M. M. Vopson, *Sol. Stat. Commun.* **152**, 2067 (2012).

²² H. Meng, B. Li, W. Ren, and Z. Zhang, *Phys. Lett. A* **377**, 567 (2013).

²³ X. Moya, S. Kar-Narayan, and N. Mathur, *Nature Mater.* **13**, 439 (2014).

²⁴ A. Fujita, K. Fukamichi, M. Yamada, and T. Goto, *J. Appl. Phys.* **93**, 7263 (2003).

²⁵ A. Fujita, S. Fujieda, K. Fukamichi, H. Mitamura, and T. Goto, *Phys. Rev. B* **65**, 014410 (2001).

²⁶ J. Lyubina, K. Nenkov, L. Schultz, and O. Gutfleisch, *Phys. Rev. Lett.* **101**, 177203 (2008).

²⁷ M. P. Annaorazov, S. A. Nikitin, A. L. Tyurin, K. A. Asatryan, and S. K. Dovletov, *J. Appl. Phys.* **79**, 1689 (1996).

²⁸ M. Annaorazov, S. Nikitin, A. Tyurin, S. Akopyan, and R. Myndyev, *Phys. Stat. Sol. (a)* **194**, 304 (2002).

²⁹ E. Vives, T. Castán, and A. Planes, *Am. J. Phys.* **65**, 907 (1997).

³⁰ C. Triguero, M. Porta, and A. Planes, *Phys. Rev. B* **76**, 094415 (2007).

³¹ C. Bean and D. Rodbell, *Phys. Rev.* **126**, 104 (1962).

³² H. Yamada, K. Fukamichi, and T. Goto, *Phys. Rev. B* **65**, 024413 (2001).

³³ P. von Ranke, N. de Oliveira, and S. Gama, *J. Magn. Magn. Mat.* **277**, 78 (2004).

³⁴ P. J. von Ranke, S. Gama, A. A. Coelho, A. de Campos, A. M. Carvalho, , F. C. G. Gandra, and N. A. de Oliveira, *Phys. Rev. B* **73**, 014415 (2006).

³⁵ P. J. von Ranke, N. A. de Oliveira, B. P. Alho, E. J. R. Plaza, V. S. R. Sousa, L. Caron, and M. S. Reis, *J. Phys.: Condens. Matter.* **21**, 056004 (2009).

³⁶ E. Z. Valiev, *Phys. of Sol. Stat.* **56**, 47 (2014).

³⁷ N. Menyuk, J. A. Kafalas, K. Dwight, and J. B. Goodenough, *Phys. Rev.* **177**, 942 (1969).

³⁸ A. Planes, T. Castán, and A. Saxena, *Phil. Mag.* **94**, 1893 (2014).

³⁹ It can be obtained from a Landau expansion of the free energy (12) and then require that the harmonic coefficient be equal to zero.

⁴⁰ C. Kittel, *Phys. Rev.* **120**, 335 (1960).

⁴¹ The phase diagram in the region corresponding to $\alpha_2^* < 0$ is specularly similar with respect to $\alpha_2^* = 0$.

⁴² It can be easily derived by imposing that the energy of both \mathcal{F} and \mathcal{AF} phases be equal at $T = 0K$.

⁴³ S. Jin, T. H. Tiefel, M. McCormack, R. A. Fastnacht, R. Ramesh, and L. H. Chen, *Science* **264**, 413 (1994).

⁴⁴ P. Schiffer, A. P. Ramirez, W. Bao, and S.-W. Cheong, *Phys. Rev. Lett.* **75**, 3336 (1995).

⁴⁵ M. Nicastro and C. H. Patterson, *Phys. Rev. B* **65**, 205111 (2002).

⁴⁶ J. M. DeTeresa, M. R. Ibarra, J. Blasco, J. García, C. Marquina, P. A. Algarabel, Z. Arnold, K. Kamenev, C. Ritter, and R. von Helmolt, *Phys. Rev. B* **54**, 1187 (1996).

⁴⁷ Y. Sun, J. Kamarad, Z. Arnold, Z. Kou, and Z. Cheng, *Appl. Phys. Lett.* **88**, 102505 (2006).

⁴⁸ Y. Sun, X. Xu, and Y. Zhang, *J. Mag. Magn. Mater.* **219**, 183 (2000).

⁴⁹ X. X. Zhang, J. Tejada, Y. Xin, G. F. Sun, K. W. Wong, and X. Bohigas, *Appl. Phys. Lett.* **69**, 3596 (1996).

⁵⁰ A. Ulyanov, Y. Kang, and S. Yoo, *J. Appl. Phys.* **103**, 07B328 (2008).

⁵¹ Z. B. Guo, Y. W. Du, J. S. Zhu, H. Huang, W. P. Ding, and D. Feng, *Phys. Rev. Lett.* **78**, 1142 (1997).

⁵² P. G. Radaelli, D. E. Cox, M. Marezio, S.-W. Cheong, P. E. Schiffer, and A. P. Ramirez, *Phys. Rev. Lett.* **75**, 4488 (1995).

⁵³ F. Hu, B. Shen, J. Sun, Z. Cheng, G. Rao, and X. Zhang, *Appl. Phys. Lett.* **78**, 3675 (2001).

⁵⁴ J. Kouvel, *J. Appl. Phys.* **37**, 1257 (1966).

⁵⁵ M. E. Gruner, E. Hoffmann, and P. Entel, *Phys. Rev. B* **67**, 064415 (2003).

⁵⁶ R. Barua, F. Jimnez-Villacorta, and L. H. Lewis, *Appl. Phys. Lett.* **103**, 102407 (2013).

⁵⁷ J. B. Staunton, R. Banerjee, M. dos Santos Dias, A. Deak, and L. Szunyogh, *Phys. Rev. B* **89**, 054427 (2014).

⁵⁸ L. M. Sandratskii and P. Mavropoulos, *Phys. Rev. B* **83**, 174408 (2011).

⁵⁹ E. G. Ponyatovskii, A. R. Kutsar, and G. T. Dubovka, *Sov. Phys. -Crystallogr.* **12**, 79 (1968).

⁶⁰ A. J. Heeger, *J. Appl. Phys.* **41**, 4751 (1970).

⁶¹ G. Dobovka, *J. Exper. Theor. Phys.* **38**, 1140 (1974).

⁶² L. I. Vinokurova, A. V. Vlmov, and M. Pardavi-Horvá, *phys. stat. sol. (b)* **78**, 353 (1976).

⁶³ M. E. Gruner and P. Entel, *Phase Transitions* **78**, 209 (2005).

⁶⁴ J. Kudrnovský, V. Drchal, and I. Turek, *Phys. Rev. B* **91**, 014435 (2015).

⁶⁵ D. W. Cooke, F. Hellman, C. Baldasseroni, C. Bordel, S. Moyerman, and E. E. Fullerton, *Phys. Rev. Lett.* **109**, 255901 (2012).